

Evaluation protocol for revealing magnonic contrast in STXM-FMR measurements

Benjamin Zingsem^{1,2}, Thomas Feggeler¹, Ralf Meckenstock¹, Taddäus Schaffers³, Santa Pile³, Hendrik Ohldag⁴, Michael Farle¹, Heiko Wende¹, Andreas Ney³, Katharina Ollefs¹

¹Faculty of Physics and Center for Nanointegration (CENIDE), University Duisburg-Essen, 47057 Duisburg, Germany,

²Ernst Ruska Centre for Microscopy and Spectroscopy with Electrons and Peter Grünberg Institute, Forschungszentrum Jülich GmbH, 52425 Jülich, Germany

³Institut für Halbleiter- und Festkörperphysik, Johannes Kepler Universität, 4040 Linz, Austria

⁴SLAC National Accelerator Laboratory, 94025 Menlo Park, CA, United States

Abstract We present a statistically motivated method to extract magnonic contrast from STXM-FMR measurement with microwave frequencies of the order of 10 GHz. With this method it is possible to generate phase and amplitude profiles with a spatial resolution of about 30 nm given by the STXM resolution, furthermore this method allows for a rigorous transformation to reciprocal \vec{k} -space, revealing \vec{k} -dependent magnon properties.

Introduction Collective oscillatory spin states, called magnons, can be excited in magnetic materials at microwave frequencies. Their spectral characteristics are determined by, and serve as a characterization method for, all magnetic parameters in a magnetic system [1]. Magnons can be used as carriers of information in data processing, such as quantum computing and spin-wave logic [2, 3, 4], with the potential to supersede conventional electronics in many ways. Various established techniques are employed for measuring magnonic excitations, the most prominent ones being Ferromagnetic Resonance (FMR)[5] and Brillouin light scattering (BLS)[6], also neutron scattering [7, 8], SEM with polarization analyzer (SEMPA)[9] and spin polarized scanning tunneling microscopy (SP-STM)[10], to name a few. FMR spectroscopy is used to investigate spectral properties, while BLS is a surface sensitive technique to measure the spatial distribution of spinwaves down to the resolution limit of visible light [6].

The technique of which we discuss the extraction of spatially resolved amplitude and phase of magnons is a combination of Scanning Transmission X-Ray Microscopy (STXM) with FMR. Here the effect of X-ray Magnetic Circular Dichroism (XMCD) is used, where the scattering of circular polarized X-Ray with electrons in a material is dependent on the spin of the electrons involved, i.e. the occupation of minority and majority spin channels in the electron density of states. In the following we discuss an evaluation technique to extract magnonic information from such measurements. This includes spectral and spatial resolution of magnonic eigenstates in real and reciprocal space, previously not attained.

Main Body

Experimental setup and Measurement technique The experimental setup combining a Ferromagnetic Resonance spectrometer and a Scanning Transmission X-Ray Microscope allows the element specific and time resolved characterization of magnetization dynamics with high spatial resolution [11] of the order of 30 nm. Using X-ray magnetic circular dichroism (XMCD) a contrast proportional to the difference in the number of minority and majority spins at the 3d orbitals is detected. For this purpose circular polarized X-rays

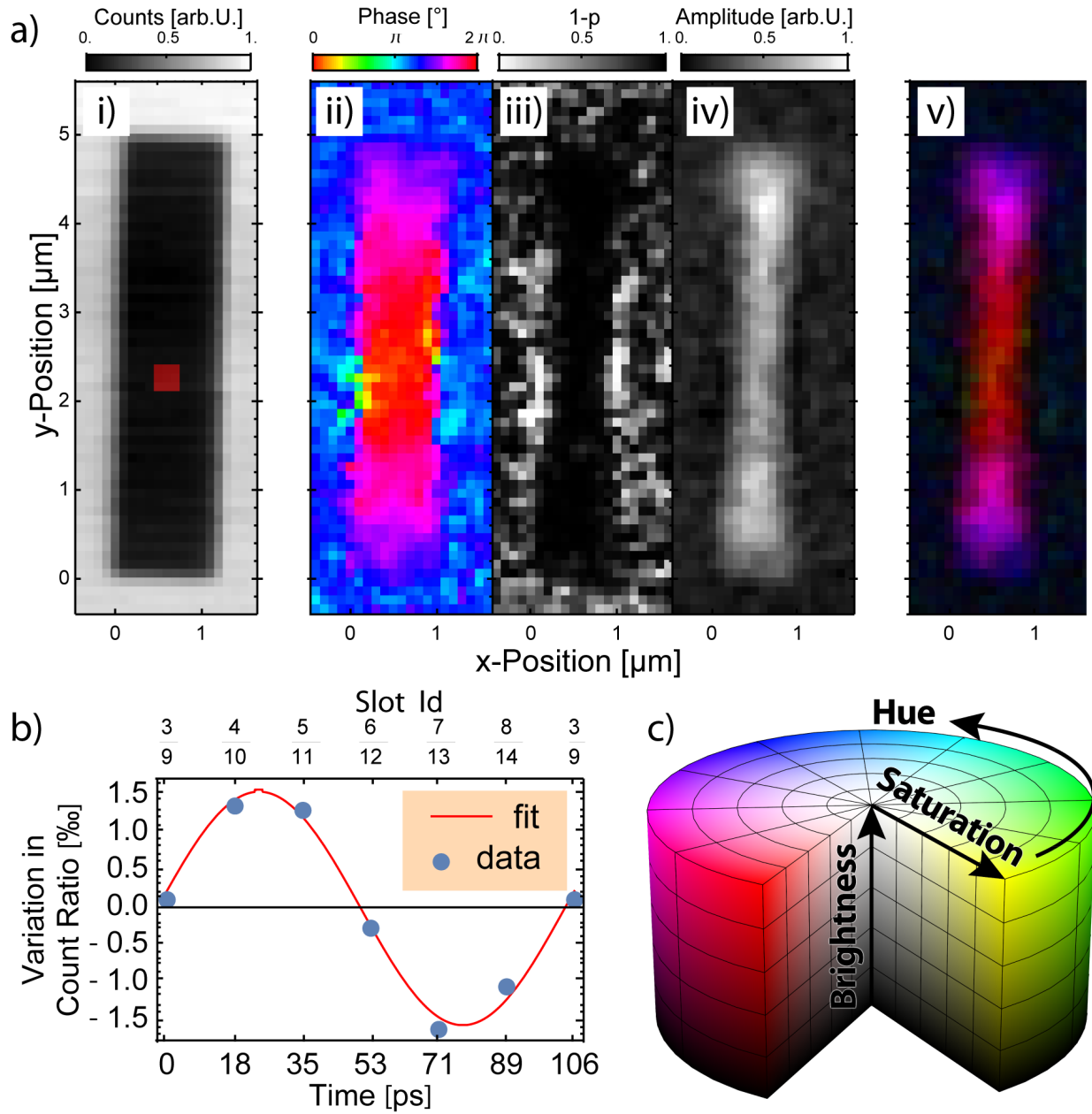


Fig. 1: Magnonic contrast image: a) i) Depiction of the X-Ray transmission count rate across the sample. ii) - iv) color channels used to encode magnonic information, where ii) depicts the phase distribution encoded as the cyclic hue channel, iii) represents the p-value of the statistical analysis at each pixel, encoded as the saturation and iv) represents the spin-wave amplitude encoded as the brightness value in v). v) Assembled HSB image of the magnonic excitation. b) time dependent recording acquired in the red region in the center of a)i). c) Three dimensional representation of the HSB color scale as used in a)v).

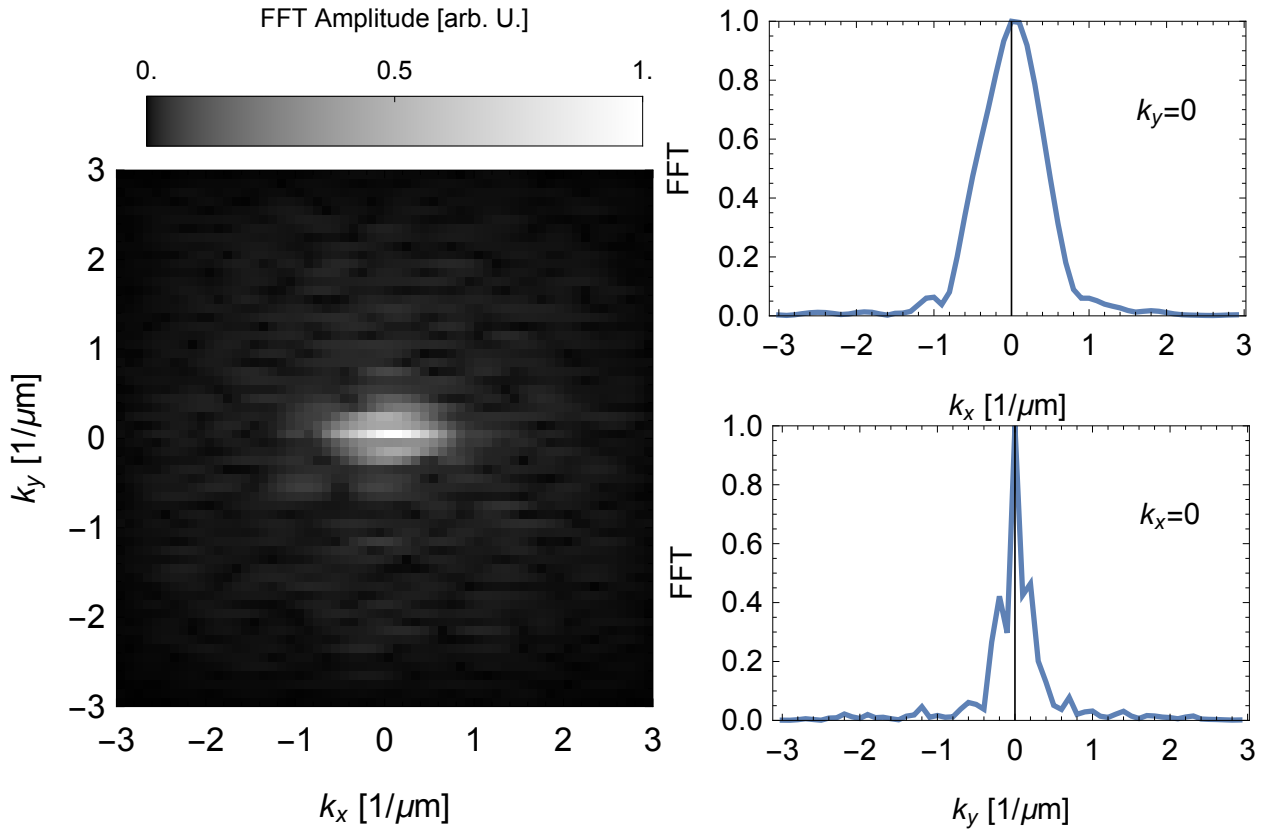


Fig. 2: Spatial Fourier transformation of the phase and amplitude values depicted in Fig. figure 1 a)ii) and a)iv). The k_x dependence shows a broad distribution around $k_x = 0$ which is most likely dominated by the spatial confinement of the sample itself. The k_y distribution on the other hand shows a narrow distribution around $k_y = 0$ with two distinct modes visible at $k_y = \pm 0.2 \mu\text{m}^{-1}$ which demonstrates that the observed oscillation is composed of two counter-propagating waves with a wavelength of about $5 \mu\text{m}$.

are focused on the sample using a zone plate. The transmitted X-rays are detected by an X-ray avalanche photodiode, located behind the sample. A static magnetic field is applied perpendicular to the wavevector of the X-rays. The sample itself is positioned in a micro resonator[12] and a microwave magnetic field is applied perpendicular to the static field and parallel the X-Ray propagation direction. The microwave frequency is synchronized to the klystron frequency of the synchrotron (SSRL: 476.315 MHz). In this case a microwave frequency of 9.446 GHz is selected, which corresponds to the 20th harmonic of the klystron frequency subtracted by 1/6, (see [11] for details). Using this setup we are detecting 6 points in time of a microwave cycle with a time distance of 18 ps, each of the points is measured with microwave on/off respectively with the same electron bunch. As the frequency of the electron bunches (bunch length of 50 ps) in the storage ring of the synchrotron is 1.28 MHz, a rectangular modulation of the microwaves is implemented at this frequency using a PIN diode, attenuating the microwaves by -35 dB. The data received from the X-ray diode is stored in a device providing 12 *slots*, the first 6 of which record the signal with microwaves turned on, whereas the X-Ray signal with microwaves turned off is stored in the remaining 6 slots [11].

The data used in this work, to demonstrate our optimized evaluation protocol has been obtained for a sample which consists of two Py stripes in a T-shape arrangement, spaced 2 μm apart. Each stripe has lateral dimensions of 5 μm by 1 μm and a thickness of 30 nm.

Evaluation method To extract time dependent oscillations in the MW-On state, the count rate in the MW-Off state has to be compared to that in the MW-On state at each position as a means of normalization. It becomes apparent that the results will be similar regardless whether ratio or difference of ON/OFF states is used to compare those, when considering

$$\frac{a_{x,y}(t)}{b_{x,y}(t)} = \frac{a_{x,y}(t) - b_{x,y}(t)}{b_{x,y}(t)} + 1 \quad (1)$$

where $a_{x,y}(t)$ is the count rate at pixel x, y and time t in the MW-On state and similarly $b_{x,y}(t)$ is the count rate in the MW-Off state. It can be motivated that the count rate without MW $b_{x,y}(t) = b_{x,y}$ is roughly constant in time as no spin waves are pumped. From that with eq. 1 the proportionality

$$\frac{a_{x,y}(t)}{b_{x,y}(t)} \propto a_{x,y}(t) - b_{x,y}(t) \quad (2)$$

follows. The influence of noise (or signal other than the desired magnonic contrast), however, is vastly different when comparing ratio and difference as a means of relating the signals. This can be estimated through the gradient of the left and right side of eq. 2 in the quantities a and b where

$$\nabla_{a,b} \left(\frac{a}{b} \right) = \begin{pmatrix} \frac{1}{b} \\ -\frac{a}{b^2} \end{pmatrix} \quad (3)$$

$$\nabla_{a,b} (a - b) = \begin{pmatrix} -b \\ a \end{pmatrix}. \quad (4)$$

Hence, fluctuations in b have a non-linear effect on fluctuations in the ratio, whereas fluctuations in a and b have a linear effect on fluctuations in the difference. Thus, the signal to noise ratio should be considered when deciding how to compare MW-On and MW-Off signal. Except for the perceived noise level, these operations yield equivalent results in the evaluation of magnonic contrast and both can be used in quantitative analysis as one can be transformed into the other using eq. 1.

A sin like magnonic response to the sin like microwave excitation is expected, such that the magnonic contrast can now be extracted by fitting a sin-function to the time dependent data at each point on the sample that was normalized using one of the aforementioned methods. Also it is expected that the dynamic response of the sample oscillates at the same frequency as the microwave driving it. Figure 1 b) depicts a sine wave fitted into the time dependent signal at one point on the sample. The model is given as

$$A \sin \left(2\pi \frac{\omega}{\omega_0} t + \phi \right) + d \quad (5)$$

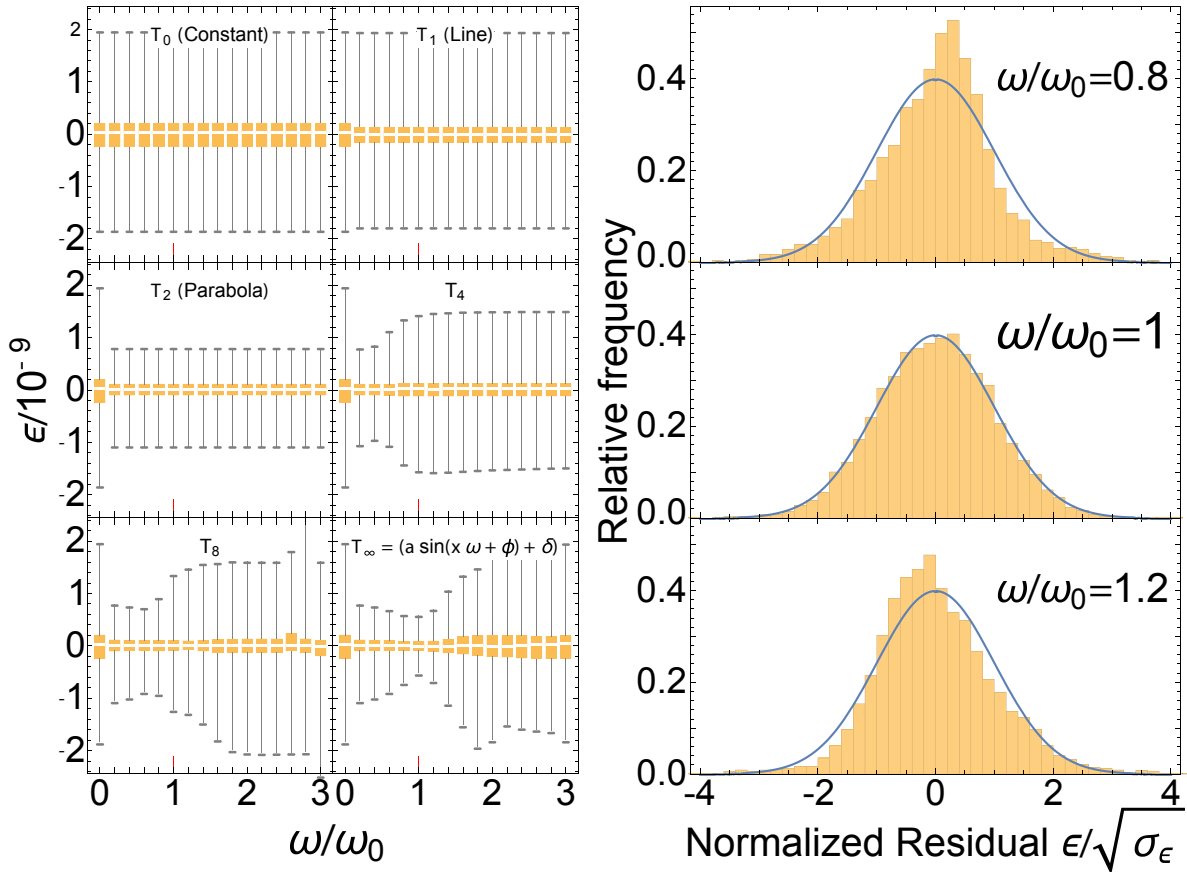


Fig. 3: Analysis of fit residuals: In this Graphic the concatenated residuals of the fits performed at each pixel in Fig. 1 are analyzed. To the left, the distribution of residuals ϵ is shown in form of a Box-Chart for various fit models as a function of the frequency. The Orange Boxes indicate the margin in which half of the residuals are scattered, with a bright line near the center marking the median. The gray lines mark the position of minimal and maximal value of the residuals. To the right, the distribution of normalized residuals for the sin model (Eq. 5) is depicted as a histogram. The normalization factor $\sqrt{\sigma_\epsilon}$ was calculated as the variance across the residuals. The orange bars mark the relative count rate for each value in the set of residuals. The blue curve is a Gaussian distribution of the form $\frac{1}{\sqrt{2\pi}} \exp\left(-\frac{x^2}{2}\right)$. A clear convergence to a narrow distribution is observed for the sine model at $\omega = \omega_0$. Simultaneously the shape of the distribution of residuals near that value closely approximates a Gaussian distribution. This would be expected if the residuals are the result of random deviations or noise. Thus we can conclude that no additional signals are present in the observed data and that there is no polynomial function with three or fewer variables, that has more explanatory power than the sine model (Eq. 5).

where A accounts for an amplitude of the oscillation, ω_0 is the excitation frequency, t is the time in periods, ϕ accounts for a phase shift relative to $t = 0$ and d describes an offset, which is usually close to 0 for the case of $a - b$ and close to 1 when analyzing $\frac{a}{b}$. Note that only A , ϕ and d are free parameters in the fit, and the physical assumption is that $\omega = \omega_0$.

Performing this fit at each pixel, we can now extract the spatial distribution of the fit parameters, i.e. the spatial distribution of amplitude and phase. Additionally a simple measure for the validity of this fit can be given by the statistical p-value. It measures the likelihood that the data-set to which the fit was applied originates from a random distribution rather than a distribution following the assumed model. The p-value therefore gives a measure for how adequate our fit is at each pixel, where small p-values indicate a good fit. These three values can then be encoded in an image as seen in Fig. 1 a)v). Here the *hue*, *saturation*, *brightness* (HSB) color scale was used, where the phase was encoded into the *hue* channel, the amplitude was encoded into the *brightness* channel, and one minus the p-value ($1 - p$) was encoded into the saturation. Thus bright pixels correspond to high amplitudes, while highly saturated pixels correspond to a very sine-like oscillation. One can quickly spot, that encoding this information into an image like this immediately reveals the spatial structure of the excited magnonic eigenstate, including phase information. The next task is to investigate the \vec{k} -vectors this state comprises. This can be achieved, by introducing a complex value $z_{x,y}$ at each pixel x, y , where $\|z_{x,y}\| = A$ and $\arg(z_{x,y}) = \phi$. Applying a Fourier transformation in the spatial coordinates x and y then transforms the spatial wave to reciprocal space, revealing the \vec{k} -vectors involved in this state. Figure 2 illustrates the \vec{k} resolution for the spatial eigenstate observed in 1. The broad distribution around $\vec{k}_x = 0$ can be attributed to the spatial confinement of the sample, while the narrow distribution around $\vec{k}_y = 0$ shows distinct maxima for the involved \vec{k} -vectors assembling the eigenmode along the long axis of the stripe.

In the previous section it was physically motivated, to assume a sine-function as representative for the investigated oscillations, one could argue, that this motivation is weak, as there may, for example, be multiple sine functions (i.e. Fourier components) involved in one oscillation, or that the data does not represent a sine function at all, but rather a simpler function. A simple test can now be performed by assuming different values for ω . Figure 3 shows the distribution of fit residuals under variation of ω , starting from $\omega = 0$ to $\omega = 2\omega_0$ in steps of $0.1\omega_0$. It is immediately apparent, that the residuals converge to a narrow Gaussian distribution at $\omega = \omega_0$ confirming the assumed frequency. Further still, the model itself can be motivated, by trying simpler functions as models for the fit. For this purpose, we considered a Taylor expansion of the sine function. This yields a set of polynomials, starting from 0th order and progressively approaching the sine function where T_n denotes a Taylor series expansion to the n th order. The residuals as a function of the frequency for various polynomials in this series are depicted in Fig. 3. It is quickly noted, that the convergence is best in only one case, namely when using the sine-function with an assumed frequency of $\omega = \omega_0$. In this case the residuals closely approximate a Gaussian distribution indicating that they are randomly distributed and not the result of a systematic deviation.

Summary We have demonstrated, how magnonic contrast can be extracted from STXM-FMR measurements with statistical rigor even in the case of few time steps. Not only frequency and spatial phase-and-amplitude profiles can be extracted, but a transposition to reciprocal space can be performed to identify the prevailing \vec{k} -vectors in a collective magnonic eigenstate. Furthermore, we have shown that our method is – beyond its physical motivation – statistically motivated, independent of physical assumptions. It carries statistical significance and allows quantitative deductions about the magnonic properties.

References

- [1] Farle M. Ferromagnetic resonance of ultrathin metallic layers. Reports on Progress in Physics. 1998;61(7):755. Available from: <http://stacks.iop.org/0034-4885/61/i=7/a=001>.
- [2] Khitun A, Bao M, Wang KL. Magnonic logic circuits. Journal of Physics D: Applied Physics. 2010;43(26):264005. Available from: <http://stacks.iop.org/0022-3727/43/i=26/a=264005>.

-
- [3] Grundler D. Reconfigurable magnonics heats up. *Nature Physics*. 2015 Jun;11:438 EP –. Available from: <https://doi.org/10.1038/nphys3349>.
- [4] Chumak AV, Vasyuchka VI, Serga AA, Hillebrands B. Magnon spintronics. *Nature Physics*. 2015 Jun;11:453 EP –. Review Article. Available from: <https://doi.org/10.1038/nphys3347>.
- [5] Vonsovskii SV. *The Phenomenon of Resonant Absorption of a High-Frequency Magnetic Field in Ferromagnetic Substances*. Oxford, London, Edinburgh, New York, Toronto, Paris, Frankfurt: Pergamon Press; 1966.
- [6] Demokritov SO, Hillebrands B, Slavin AN. Brillouin light scattering studies of confined spin waves: Linear and nonlinear confinement. *Physics Reports*. 2001;348:441–489.
- [7] Izyumov Y, Ozerov RP. *Magnetic Neutron Diffraction*. New York: Plenum Press; 1970.
- [8] Chatterji T. *Neutron Scattering from Magnetic Materials*. Amsterdam, Boston, Heidelberg, London, New York, Oxford, Paris, San Diego, San Francisco, Singapore, Sydney, Tokyo: Elsevier; 2006.
- [9] Koike K, Hayakawa K. Scanning Electron Microscope Observation of Magnetic Domains Using Spin-Polarized Secondary Electrons. *Japanese Journal of Applied Physics*. 1984 mar;23(Part 2, No. 3):L187–L188. Available from: <https://doi.org/10.1143%2Fjap.23.1187>.
- [10] Balashov T, Takács AF, Wulfhekel W, Kirschner J. Magnon Excitation with Spin-Polarized Scanning Tunneling Microscopy. *Phys Rev Lett*. 2006 Nov;97:187201. Available from: <https://link.aps.org/doi/10.1103/PhysRevLett.97.187201>.
- [11] Bonetti S, Kukreja R, Chen Z, Spoddig D, Ollefs K, Schöppner C, et al. Microwave soft x-ray microscopy for nanoscale magnetization dynamics in the 5–10 GHz frequency range. *Review of Scientific Instruments*. 2015;86(9):093703.
- [12] Narkowicz R, Suter D, Stonies R. Planar microresonators for EPR experiments. *Journal of Magnetic Resonance*. 2005;175(2):275–284.